



**HAL**  
open science

## Decadal increase in Arctic dimethylsulfide emission

Martí Galí, Emmanuel Devred, Marcel Babin, Maurice Levasseur

► **To cite this version:**

Martí Galí, Emmanuel Devred, Marcel Babin, Maurice Levasseur. Decadal increase in Arctic dimethylsulfide emission. *Proceedings of the National Academy of Sciences of the United States of America*, 2019, 116 (39), pp.19311-19317. 10.1073/pnas.1904378116 . hal-03044166

**HAL Id: hal-03044166**

**<https://hal.science/hal-03044166>**

Submitted on 5 Jan 2021

**HAL** is a multi-disciplinary open access archive for the deposit and dissemination of scientific research documents, whether they are published or not. The documents may come from teaching and research institutions in France or abroad, or from public or private research centers.

L'archive ouverte pluridisciplinaire **HAL**, est destinée au dépôt et à la diffusion de documents scientifiques de niveau recherche, publiés ou non, émanant des établissements d'enseignement et de recherche français ou étrangers, des laboratoires publics ou privés.

# Decadal increase in Arctic dimethylsulfide emission

Martí Galí<sup>1</sup>, Emmanuel Devred<sup>2</sup>, Marcel Babin<sup>3</sup>, Maurice Levasseur<sup>1</sup>

<sup>1</sup>Laval University, <sup>2</sup>Bedford Institute of Oceanography, <sup>3</sup>Université Laval

Submitted to Proceedings of the National Academy of Sciences of the United States of America

**Dimethylsulfide (DMS), a gas produced by marine microbial food webs, promotes aerosol formation in pristine atmospheres, altering cloud radiative forcing and precipitation. Recent studies suggest that DMS controls aerosol formation in the summertime Arctic atmosphere and call for an assessment of pan-Arctic DMS emission (EDMS) in a context of dramatic ecosystem changes. Using a new remote sensing algorithm, we show that summertime EDMS from ice-free waters increased at a mean rate of  $13.3 \pm 6.7$  Gg S decade<sup>-1</sup> ( $\sim 33\%$  decade<sup>-1</sup>) north of 70°N between 1998 and 2016. This trend, mostly explained by the reduction in sea ice extent, is consistent with independent atmospheric measurements showing an increasing trend of methane sulfonic acid, a DMS oxidation product. Extrapolation to an ice-free Arctic summer could imply a 2.4-fold ( $\pm 1.2$ ) increase in EDMS compared to present emission. However, unexpected regime shifts in Arctic geo- and ecosystems could result in future EDMS departure from the predicted range. Superimposed on the positive trend, EDMS shows substantial interannual changes and non-monotonic multiyear trends, reflecting the interplay between physical forcing, ice retreat patterns and phytoplankton productivity. Our results provide key constraints to determine whether increasing marine sulfur emissions, and resulting aerosol-cloud interactions, will moderate or accelerate Arctic warming in the context of sea ice retreat and increasing low-level cloud cover.**

Dimethylsulfide | Arctic | Plankton | Sea-ice | Aerosols

## Introduction

The Arctic region is warming more than two times faster than the global average, and ice-free summers could be a reality in the next few decades (1). Removal of the ice barrier boosts ocean-atmosphere exchanges of energy, gases and particles, with profound effects on marine ecosystems and climate. Enhanced heat and moisture fluxes are increasing the abundance of low-level clouds (2) and, very likely, the prevalence of liquid-state clouds and precipitation (3). Ice retreat allows more solar radiation to penetrate into the ocean surface, driving a pan-Arctic increase in phytoplankton primary production (2, 4–6). Meanwhile, changes in stratification and nutrient supply to the sunlit ocean layer modulate phytoplankton productivity (4–7) and alter phytoplankton bloom phenology (7–10) and the occurrence of species with distinct biogeochemical traits (10–12) such as their capacity to produce the climate active gas DMS (13, 14). DMS is produced through microbial decomposition of dimethylsulfoniopropionate (DMSP), a compound synthesized in variable amounts by different phytoplankton groups (13, 14). Despite complex biogeochemical cycling (14, 15), high-latitude DMS production scales to first order with phytoplankton biomass and productivity over the seasonal cycle at large scales (16–19). In a scenario of changing ice cover and phytoplankton dynamics, changes in the magnitude, timing and spatial distribution of Arctic DMS emission (EDMS) are expected (14, 20, 21).

Previous estimates of Arctic Ocean EDMS have been made using either sea-surface DMS climatologies (16), produced through interpolation of sparse in situ data, or prognostic models (20, 21). Both types of estimates depict the Arctic as a region with relatively low sea-air DMS flux per unit area (FDMS) on an annual basis (mean FDMS lower than  $2 \mu\text{mol m}^{-2} \text{d}^{-1}$ ) compared to temperate and tropical oceans (mean FDMS of about 4–5

$\mu\text{mol m}^{-2} \text{s}^{-1}$ ) (16, 20). However, Arctic FDMS is concentrated in the short productive summer season, and relatively high daily fluxes have been reported associated to phytoplankton blooms that form in the wake of melting sea ice, often exceeding  $10 \mu\text{mol m}^{-2} \text{s}^{-1}$  (14, 15, 20). Ice margin phytoplankton blooms are a major feature of the Arctic ecosystem. They typically last for 1–3 weeks after ice break-up and are promptly detected using ocean color remote sensing (8, 9, 23). Given the patchy and ephemeral nature of Arctic EDMS, accurate estimates of its magnitude and spatial-temporal distribution based on climatological datasets are severely limited.

Once emitted to the atmosphere, the influence of DMS on atmospheric particles does not depend strictly on the magnitude of FDMS. Rather, it is the background concentration of aerosol particles that critically determines whether atmospheric DMS oxidation products can nucleate new particles or condense onto pre-existing ones (24–26). In summer, different processes isolate the Arctic marine boundary layer from southern aerosol sources (both natural and anthropogenic), namely: the northward migration of the atmospheric polar front, the efficient wet scavenging by drizzling stratocumulus clouds, and the formation of surface inversion layers (3, 26, 27). These processes result in extremely low aerosol concentrations, which favor new particle formation from local gaseous precursors (24, 26, 28, 29). Recent measurements and associated modeling have shown instances where DMS controls the formation of ultrafine particles (24, 29), which can grow large enough to act as cloud condensation nuclei (CCN) (24, 26). Thus, changes in Arctic Ocean EDMS could alter aerosol populations, light scattering and cloud-seeding activity (27, 28, 30, 31), and hence the capacity of clouds to reflect incoming radiation

## Significance

**As Arctic sea-ice cover declines because of climate warming, the emission of reactive gases produced by marine microbes increases. One of such gases, dimethylsulfide, forms new atmospheric particles that contribute to cloud formation. This can either cool the Earth's surface by reflecting incoming sunlight, or warm it due to the blanket effect. Here we quantify for the first time Arctic Ocean dimethylsulfide emission between 1998 and 2016 using satellite observations of microalgal biomass and physical variables. We report an increasing trend, driven by sea-ice loss, and substantial year-to-year variability modulated by biological productivity. Our results can help understand the impacts and feedbacks of marine plankton on Arctic climate and foresee their future trajectories under the pressure of global change.**

## Reserved for Publication Footnotes

137  
138  
139  
140  
141  
142  
143  
144  
145  
146  
147  
148  
149  
150  
151  
152  
153  
154  
155  
156  
157  
158  
159  
160  
161  
162  
163  
164  
165  
166  
167  
168  
169  
170  
171  
172  
173  
174  
175  
176  
177  
178  
179  
180  
181  
182  
183  
184  
185  
186  
187  
188  
189  
190  
191  
192  
193  
194  
195  
196  
197  
198  
199  
200  
201  
202  
203  
204

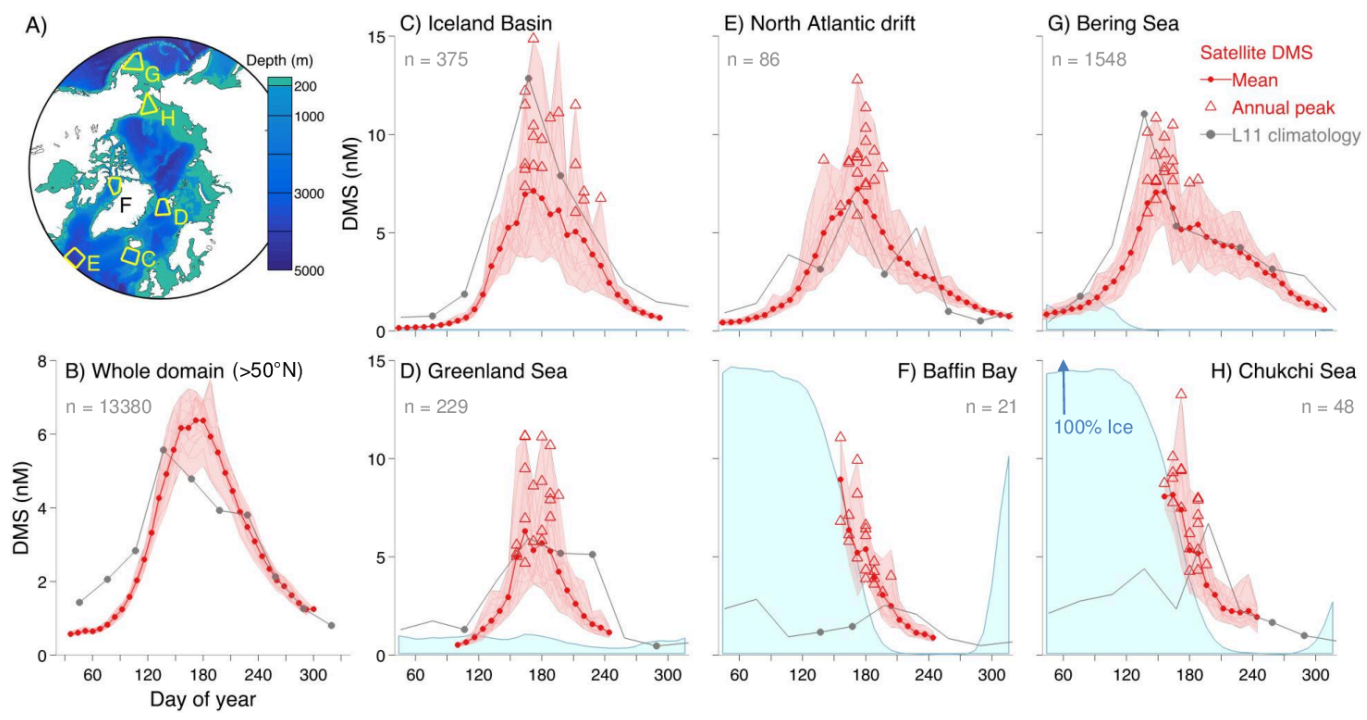


**Fig. 1. DMS seasonal cycles in Subarctic and Arctic seas.** A) Bathymetric map and ecoregions (yellow polygons) used to illustrate DMS dynamics; B-H) mean DMS seasonal cycle derived from the satellite algorithm (thick red line) and from the L11 climatology (thick grey line) for latitudes higher than 50°N (B) and six smaller ecoregions (C-H) shown in panel (A). In the satellite seasonal cycles (C-H), light red lines mark individual years, light red shadow marks the 19-years envelope, and red triangles mark the annual peak for each year. In the monthly L11 climatology, markers indicate that in situ data was available in a given month, whereas no marker indicates that monthly DMS was estimated through interpolation. The numbers in grey indicate the amount (n) of in situ measurements available to calculate the L11 climatology in a given ecoregion (1979-2010). The light blue shade is the mean fractional ice cover, scaled to the maximum of the y-axis, shown only for regions within the seasonal ice zone. Analogous plots for FDMS are shown in Fig. S6.

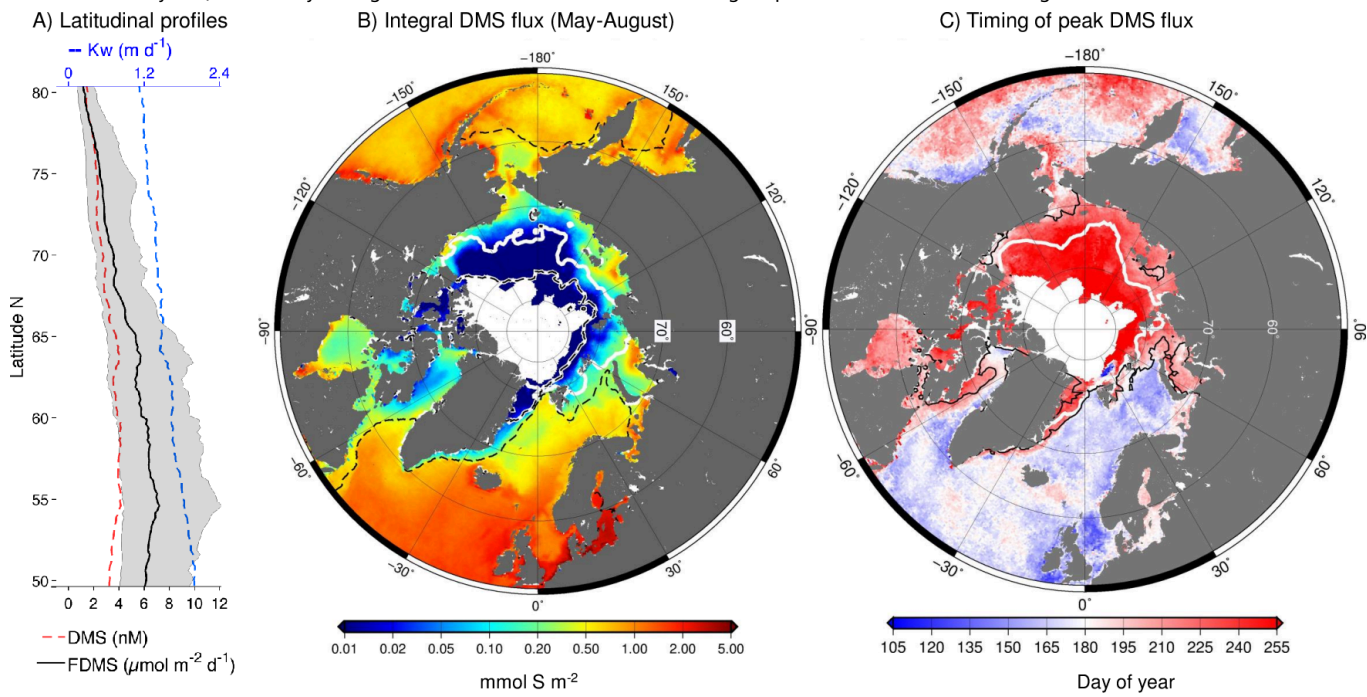


**Fig. 2. Spatial distribution and timing of summertime DMS emission in May through August, 2003-2016.** A) Median latitudinal profile in ice-free pixels of sea surface DMS concentration, sea-air flux (FDMS; interquartile range is shaded), and sea-air gas exchange coefficient ( $K_w$ ); B) integral summertime FDMS between year days 121 and 248; C) mean day of the annual peak in sea-air DMS flux. Contour lines in (B) show: 2003-2016 median of maximal late winter ice extent (black dashed line); minimal early September ice extent in 2003 (white line); minimal early September ice extent in 2012 (black dashed on white line). Contours in (C) enclose the area where: more than 50% of the summertime DMS emission occurs during a 24-day period centered on the annual peak (black line); the duration of the ice-free season is shorter than 48 days (white line) (medians of the 2003-2016 period).

205  
206  
207  
208  
209  
210  
211  
212  
213  
214  
215  
216  
217  
218  
219  
220  
221  
222  
223  
224  
225  
226  
227  
228  
229  
230  
231  
232  
233  
234  
235  
236  
237  
238  
239  
240  
241  
242  
243  
244  
245  
246  
247  
248  
249  
250  
251  
252  
253  
254  
255  
256  
257  
258  
259  
260  
261  
262  
263  
264  
265  
266  
267  
268  
269  
270  
271  
272

273  
274  
275  
276  
277  
278  
279  
280  
281  
282  
283  
284  
285  
286  
287  
288  
289  
290  
291  
292  
293  
294  
295  
296  
297  
298  
299  
300  
301  
302  
303  
304  
305  
306  
307  
308  
309  
310  
311  
312  
313  
314  
315  
316  
317  
318  
319  
320  
321  
322  
323  
324  
325  
326  
327  
328  
329  
330  
331  
332  
333  
334  
335  
336  
337  
338  
339  
340

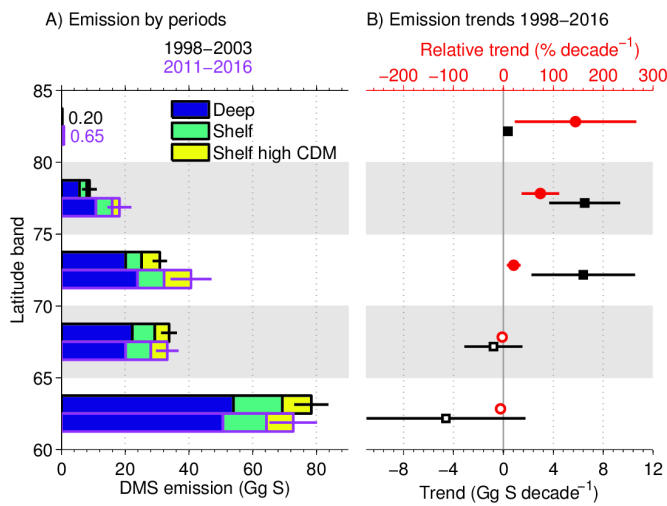


**Fig. 3. Mean zonal trends in summertime (May-August) DMS emission (EDMS).** Left: EDMS mean  $\pm$  standard deviation for 1998-2003 (black line) and 2011-2016 (grey line); emissions are broken down into deep ocean basins and continental shelves. The latter are further divided to show waters with strong riverine influence as depicted by high content of colored detrital matter (CDM) that increases uncertainty in satellite Chl retrievals. Right: EDMS trends for the period 1998-2016 (black squares), and corresponding relative increase with respect to the 1998-2003 baseline period (red circles). Filled symbols mark significant trends at 95% confidence level, and error bars show the standard error of the linear regression slope (which is sometimes smaller than the symbols).

(shortwave forcing or albedo) and trap heat (longwave forcing) (3, 25, 32-34).

To document trends in EDMS for the first time in the Arctic, we calibrated for high northern latitudes the DMS<sub>SAT</sub> algorithm (17), which estimates sea-surface DMS concentration (nM) from remotely sensed variables, chiefly chlorophyll *a* concentration (Chl), light penetration depths, and photosynthetically available radiation (PAR). We implemented and validated the algorithm at 8-day and 28-km resolution, covering a total of 19 years using data from two sensors: the Sea-viewing Wide Field-of-view Sensor (SeaWiFS, years 1998-2007), and the Moderate Resolution Imaging Spectroradiometer onboard the Aqua satellite (MODIS-Aqua, 2003-2016). This enables the exploration of interannual changes and trends in EDMS from ice-free Arctic and Subarctic waters.

**Results and Discussion**

*DMS concentration and emission patterns in northern high latitudes*

The satellite algorithm shows remarkable skill across two orders of magnitude of DMS concentration when compared to in situ data, with log<sub>10</sub> space root-mean-square error of 0.40 and Pearson's correlation coefficient of 0.64 (SI Appendix, Fig. S3). Comparison between DMS<sub>SAT</sub> results and the existing climatology based on interpolation of in situ DMS data (16) (here referred to as L11) highlights the strengths of the satellite algorithm. In areas with little or no seasonal ice cover, including three distinct ecoregions in the North Atlantic (50°N-80°N; Fig. 1C-E) and the Bering Sea (Fig. 1G), the mean DMS<sub>SAT</sub> seasonal cycle agrees well with L11 (Fig. 1). Good agreement between DMS<sub>SAT</sub> and L11 is also found for the whole study domain (latitudes >50°N; Fig. 1B). In contrast, in the seasonal ice zone, temporal (Fig. 1F and H) and spatial (SI Appendix, Fig. S4) patterns derived from DMS<sub>SAT</sub> differ markedly from the L11 climatology. In these areas, satellite-derived DMS reflects elevated concentrations (often  $\geq 5$  nM) in the wake of melting sea ice, in better accordance with several field surveys of phytoplankton blooms in the marginal ice zone (14, 15, 22). Another salient feature of DMS<sub>SAT</sub> results is the

wide interannual variability in the magnitude and timing of maximal DMS concentrations (Fig. 1C-H). None of these features can be examined using global DMS climatologies, produced through multiyear averaging, interpolation, and smoothing of sparse in situ measurements (16, 17).

We calculated sea-air DMS flux (FDMS;  $\mu\text{mol S m}^{-2} \text{d}^{-1}$ ), for ice-free waters only (<10% ice cover per pixel), using satellite DMS fields, meteorological reanalysis data and gas exchange parameterizations (SI Appendix, Fig. S5). Here, we examine large-scale FDMS patterns during the summer period, defined as May to August (year days 121 to 248), when  $\sim 70\%$  of the annual open water emission occurs. As shown in Fig. 2A, the main feature of FDMS is a marked decrease between 55°N and 80°N. This reflects the combination of three main controlling factors, all of which decrease polewards: (i) the duration of the ice-free season (4), (ii) the mean summertime DMS concentration (Fig. S4), and (3) the sea-air gas transfer coefficient ( $K_w$ ), which in turn depends on wind speed and sea-surface temperature (SST) (Fig. S5). Compared to Subarctic seas, the Arctic seasonal ice zone stands out as a region of overall low summer-integrated FDMS (Fig. 2B), concentrated during a brief period (contour lines in Fig. 2C) when FDMS can be locally high but also variable (Fig. S6). The frequency of FDMS > 10  $\mu\text{mol m}^{-2} \text{d}^{-1}$  based on satellite diagnosed DMS is 3-fold higher than that based on L11 (Fig. S6) and, unlike the latter, can reach up to 30  $\mu\text{mol m}^{-2} \text{d}^{-1}$ , in agreement with in situ studies (15, 22).

*Pan-Arctic summer DMS emission, 1998-2016*

To estimate DMS emission (EDMS), we integrated FDMS over latitudinal and bathymetric domains through the summer (May-August) period. The mean satellite-based EDMS in summer between years 1998 and 2016 was  $113 \pm 10$  and  $50 \pm 11$  Gg S for the 60-70°N and >70°N latitude bands, respectively (Fig. 3). These estimates are robust to uncertainty in satellite input data and algorithm coefficients (SI Appendix, Table S3).

Satellite-derived time series indicate that Arctic summer EDMS increased significantly between 1998 and 2016 (Fig. 3). The 70-75°N and 75-80°N latitude bands contributed most of the increase, with about 6 Gg S decade<sup>-1</sup> each (Fig. 3). In relative terms, however, this implies a faster increase in the 75-80°N band (74% decade<sup>-1</sup>) compared to the 70-75°N band (21% decade<sup>-1</sup>), with respect to the 1998-2003 baseline. A very small but significant trend of  $0.36 \pm 0.15$  Gg S decade<sup>-1</sup> is detected north of 80°N, which nonetheless corresponds to more than a doubling per decade. The total rate of increase of summer EDMS, north of 70°N, is  $13.3 \pm 6.7$  Gg S decade<sup>-1</sup>, or  $33 \pm 17\%$  decade<sup>-1</sup> (Fig. 4A). The months of June and July dominate this response ( $8.3 \pm 4.3$  Gg S decade<sup>-1</sup>). Interestingly, the positive trend north of 70°N was accompanied by a smaller non-significant decrease between 60°N and 70°N of  $-5.4 \pm 8.4$  Gg S decade<sup>-1</sup> ( $-4.8 \pm 7.5\%$  decade<sup>-1</sup>) (Fig. 3). Altogether, this reveals a poleward shift of DMS emissions.

Hitherto, the only evidence for increasing Arctic Ocean EDMS came from atmospheric measurements of methane sulfonic acid (MSA), a specific product of DMS oxidation. In three Arctic stations (Barrow, Alaska; Alert, Nunavut; Mt. Zeppelin, Svalbard), MSA concentration in aerosol samples increased at a rate of between 45% and 83% decade<sup>-1</sup> between 1998 and 2009 during July and August (31), concomitant with pronounced sea ice loss north of 70°N. Our satellite-derived EDMS estimates for the same period and months suggest an increase of 40% decade<sup>-1</sup> north of 70°N, at the lower bound of MSA rates of increase. Note however that our assessment does not include ice-infested waters, sea-ice microorganisms and melt ponds, whose EDMS could also be increasing (14). Although ice-free seawater largely dominates present-day EDMS (35, 36), better knowledge of ice-related and non-marine DMS sources is needed (36). Yet, the overall con-

341  
342  
343  
344  
345  
346  
347  
348  
349  
350  
351  
352  
353  
354  
355  
356  
357  
358  
359  
360  
361  
362  
363  
364  
365  
366  
367  
368  
369  
370  
371  
372  
373  
374  
375  
376  
377  
378  
379  
380  
381  
382  
383  
384  
385  
386  
387  
388  
389  
390  
391  
392  
393  
394  
395  
396  
397  
398  
399  
400  
401  
402  
403  
404  
405  
406  
407  
408

409  
410  
411  
412  
413  
414  
415  
416  
417  
418  
419  
420  
421  
422  
423  
424  
425  
426  
427  
428  
429  
430  
431  
432  
433  
434  
435  
436  
437  
438  
439  
440  
441  
442  
443  
444  
445  
446  
447  
448  
449  
450  
451  
452  
453  
454  
455  
456  
457  
458  
459  
460  
461  
462  
463  
464  
465  
466  
467  
468  
469  
470  
471  
472  
473  
474  
475  
476

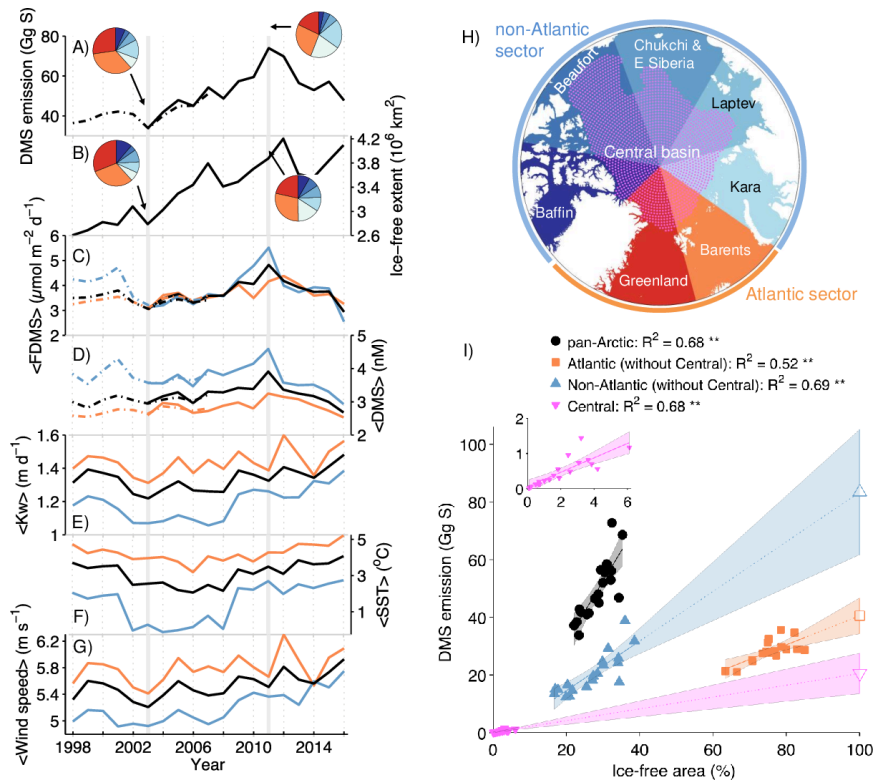


**Fig. 4. Interannual variations in DMS emission and its driving factors north of 70°N.** All panels show May-August integrals (DMS emission) or means (other variables). A) DMS emission, B) mean ice-free ocean area, C) mean FDMS, D) mean DMS concentration, E) sea-air DMS transfer coefficient ( $K_w$ ), F) sea surface temperature (SST), G) wind speed. Values in (C-G) correspond to ice-free pixels only. Different lines correspond to the whole domain >70°N and its division into two sectors: Atlantic-influenced and non-Atlantic regions, according to the map in (H). The pie charts in panels A and B illustrate the relative contribution of different source regions (colored following H) to EDMS, and their corresponding share of ice-free extent, in the years with lowest (2003) and highest (2011) EDMS. I) shows the domain-specific relationship between % ice-free extent and DMS emission. In this plot, the Central Arctic basin (pink stippling in panel H) is represented separately, and its area subtracted from the other regions to calculate the regressions. Empty symbols show extrapolation to 100% ice-free extent for the Atlantic, non-Atlantic and Central domains, and shaded areas show the 95% confidence intervals of predictions.

477  
478  
479  
480  
481  
482  
483  
484  
485  
486  
487  
488  
489  
490  
491  
492  
493  
494  
495  
496  
497  
498  
499  
500  
501  
502  
503  
504  
505  
506  
507  
508  
509  
510  
511  
512  
513  
514  
515  
516  
517  
518  
519  
520  
521  
522  
523  
524  
525  
526  
527  
528  
529  
530  
531  
532  
533  
534  
535  
536  
537  
538  
539  
540  
541  
542  
543  
544

sistency between our satellite estimates and independent MSA measurements lends confidence to the observed EDMS trends.

*Ice retreat patterns and ocean productivity control Arctic EDMS*

The 19-year EDMS time series shows three distinct periods and a non-monotonic behavior (Fig. 4A). EDMS showed small oscillations between 1998 and 2003, increased rapidly between 2003 and 2011, and decreased at a similar rate between 2011 and 2016. Between 2003 and 2011, EDMS increased by 111%, more than expected from the increase in ice-free extent alone (39%; Fig. 4B), due to a concomitant increase in mean FDMS (55%; Fig. 4C); heightened FDMS reflected, in turn, slight increases in DMS and  $K_w$  in open waters. Conversely, EDMS decreased between 2011 and 2016 owing to decreased DMS concentration in open waters, although ice-free extent showed erratic oscillations and  $K_w$  continued to increase slowly (Fig. 4E-G).

The ice-free ocean extent in summer north of 70°N increased between 1998 and 2016 at a mean rate of  $28 \pm 7\%$  per decade, with a maximum in 2012 (Fig. 4B). This trend is similar to the mean rate of increase in EDMS ( $33\%$  decade<sup>-1</sup>) and explains 68% of its interannual variance (Fig. 4I). To appraise the effect of seawater DMS variability on EDMS variability at the interannual time scale, we re-computed EDMS replacing the 19-year  $DMS_{SAT}$  time series by climatological DMS fields, while allowing sea ice, wind speed and SST to vary. In this experiment, the fraction of EDMS variance explained by ice-free extent increases from 68% to 87% (89%) using the  $DMS_{SAT}$  (L11) 8-day climatology. This exercise shows that changes in sea-surface DMS concentration (reflecting underlying ecosystem productivity) cause substantial interannual variability in FDMS and therefore in EDMS, adding to the variability arising from gas exchange coefficients (Fig. 4E-G). To further explore the interplay between ice cover and FDMS, we performed a spatial decomposition of EDMS changes over successive years (SI Appendix, Fig. S7). This analysis shows that net changes in ice-free extent and shifts in ice retreat patterns over the melt season dominated interannual changes in EDMS. Yet,

local FDMS variations contributed similarly to EDMS changes in some years, especially after 2010.

Since the Arctic Ocean comprises contrasting biogeochemical regimes (2, 4, 6, 7), regional breakdown is needed to understand the interplay between the geographic patterns of ice retreat and the drivers of EDMS. Our analysis indicates that interannual EDMS changes result from two main components (Fig. 4). On one hand, the Atlantic-influenced Greenland and Barents seas, with low or moderate ice cover, moderate productivity, and relatively high wind speed and SST (hence  $K_w$ ), generally dominated EDMS north of 70°N. These Atlantic-influenced seas displayed modest interannual variability and a smaller-than-average positive EDMS trend ( $19 \pm 10\%$  decade<sup>-1</sup> between 1998 and 2016). On the other hand, inner Arctic shelves displayed wider variability and trends, particularly the Kara and Laptev seas, owing to the convolution of large variations in ice cover distribution and sharper FDMS gradients (Fig. 2B). Extreme expression of this pattern occurred in 2003 and 2011, as illustrated with pie charts in Fig. 4. In 2003 the Atlantic sector dominated EDMS, whereas in 2011 the inner shelves dominated EDMS despite the concurrent increase in Atlantic sector emissions (SI Appendix, Fig. S8).

Modulation of Arctic EDMS by the interplay between variable ice retreat and sea-surface DMS patterns is a salient finding enabled by satellite remote sensing. The magnitude of FDMS-driven interannual variability reported here should be viewed with caution due to (i) the lack of multiyear in situ DMS time series across Arctic ecoregions, and (ii) increased  $DMS_{SAT}$  uncertainty in river outflow areas, mainly caused by uncertainty in satellite chlorophyll (note however that river outflow areas account for a minor fraction of pan-Arctic EDMS; Fig. 3A) (SI Appendix, section 5). Despite these shortcomings, the temporal trends and spatial patterns we observe are broadly consistent with those previously reported for satellite-based primary production between 1998 and 2012 (4, 6, 9) (which suffer from similar uncertainties as  $DMS_{SAT}$ ). In summary, our results suggest that the

Arctic Ocean will display substantial interannual variability and periods of transient EDMS decrease, superimposed on the robust upwards EDMS trend dictated by ice receding (Fig. 4I), during its transition to an ice-free state in summer.

#### Future scenarios

Can contemporary changes hint at the future Arctic Ocean EDMS? Extrapolation of our results to a 100% ice-free Arctic in summer implies a 2.4-fold increase in EDMS (1.2–3.6, propagated 95% CI) with respect to the 2011–2016 average, and a mean summertime EDMS of  $144 \pm 66$  Gg S north of  $70^\circ\text{N}$  (Fig. 4I). New emissions are expected to arise mostly from regions that presently have relatively high ice cover, namely the productive inner Arctic shelves. Conversely, the Atlantic sector, with low or moderate ice cover at present, is close to attaining its full EDMS potential if FDMS remains at current levels. Previous projections of EDMS suggested an increase of between 2- and 15-fold in an ice-free Arctic, and were largely sensitive to the representation of sea-surface DMS concentrations (see compilation in SI Appendix, section 7). Our satellite-based assessment, which accounts for domain-specific responses, helps constraining these projections and suggests that an increase larger than 3-fold is unlikely. This is because complete sea-ice loss from the Central Arctic basin, with heavy ice cover at present, will contribute little new EDMS due to prevailing low FDMS in satellite-observed pixels in that area (Fig. 2B).

The scenario described above is consistent with conceptual (7) and numerical (5) model predictions suggesting that salinity stratification and resulting nutrient limitation will prevent large increases in phytoplankton production in the Arctic as sea ice loss proceeds. However, our EDMS estimates for an idealized ice-free scenario suffer from multiple sources of uncertainty. First, the observed linear relationship between ice-free extent and EDMS will not necessarily hold in the future, and its extrapolation is particularly speculative in domains with high ice cover at present (Fig. 4I). In this regard, the relationship between ice cover and pan-Arctic primary production is poorly constrained in current multimodel projections (5). Second, estimation of future DMS emission is confounded by additional layers of complexity that interact with each other (14): the response of plankton communities to multiple stressors, with a potentially prominent but poorly understood role for acidification (37); the strong taxonomic dependence of DMSP synthesis; and the complex biogeochemical cycling of DMS in seawater (13, 14).

The relationship between airborne MSA and phytoplankton production in historical records could help constrain EDMS projections (14, 18, 19). MSA trapped in Greenland ice cores shows a robust positive relationship with in-situ sampled phytoplankton and satellite-observed net primary production (NPP) around southern Greenland over several decades (19). This observation supports extrapolation of the satellite-era EDMS trends. Yet, the relationship between NPP and MSA may be confounded by variable atmospheric MSA yields (14, 31) and by differences in phytoplankton taxonomy across source regions (18, 35). In the light of these findings, the response of Arctic phytoplankton to environmental forcing appears particularly critical. A warmer, more stable and irradiated water column (7, 15) might favor nanoplanktonic strong DMS producers, like coccolithophores (10) and *Phaeocystis pouchetii* (20). Such a taxonomic shift could enhance EDMS from the seasonal ice zone, offsetting other processes predicted to affect negatively EDMS, e.g. acidification (37).

Understanding and predicting how changes in marine EDMS will affect the Arctic climate requires progress in many fronts. Although atmospheric models still strive to represent aerosol (26, 27) and cloud (3, 34) dynamics, there is growing consensus that (i) DMS is an essential ingredient for Arctic marine boundary layer nucleation; and (ii) nucleation rates will increase in the future (3,

26, 27) owing to concomitant increases in atmospheric humidity, aerosol wet removal and marine aerosol precursor emissions. In line with these predictions, increasing frequency of aerosol nucleation events has been clearly linked to ice retreat at the Mt. Zeppelin observatory ( $78.9^\circ\text{N}$ ) (28).

Current knowledge suggests that CCN concentrations are unlikely to increase as much as new particle formation (nucleation) rates, due to a concomitant increase in aerosol removal (26, 27). Yet, DMS will still play a critical role in seeding and sustaining CCN populations, and could also affect precipitation (27, 38). Widening the focus, the impact of increasing EDMS on CCN populations will also depend on changing anthropogenic sulfur emissions and their transport to the Arctic. On-going reductions in power plant emissions in the northern hemisphere (39) may magnify the role of DMS or extend its seasonal dominance, unless they are compensated by increasing shipping, industrialization or oil and gas extraction in the Arctic.

The future response of cloud radiative forcing is also uncertain. Unlike in lower latitudes, low-level marine clouds in the Arctic act to retain heat in the ocean-atmosphere system during most of the year (32). Net cloud cooling is currently restricted to a short midsummer period when high solar elevation and low ice cover co-occur, but the seasonal radiation budget will change as ice recedes. Extremely low CCN concentrations that generally occur over the ice pack imply strong sensitivity to CCN changes (33), amplifying uncertainty in indirect aerosol forcing (34). An increase in CCN concentrations is generally associated with enhanced cloud albedo and a cooling effect (3, 30, 34), with recent estimates suggesting a shortwave forcing of  $-1$  to  $-2$  W  $\text{m}^{-2}$  in response to a 2- to 5-fold increase in Arctic EDMS (3) (SI Appendix). However, a CCN increase might also enhance longwave cloud forcing over the CCN-depleted pack ice (33). This response is poorly quantified and could offset shortwave forcing, causing net warming and further accelerating ice melt (26, 28).

Our study highlights the key role of atmospheric forcing in driving Arctic EDMS through the control of ice retreat (40), plankton dynamics (7, 14) and gas exchange. Since large-scale weather systems also determine air-mass transport pathways (26), the fate of atmospheric DMS and its interaction with aerosols and clouds cannot be fully understood by analyzing climatological fields in the variable and heterogeneous Arctic environment. The space- and time-resolved FDMS estimates presented here provide a key constraint for atmospheric models and can help reduce uncertainty in projections of aerosol direct and indirect forcing (3, 27, 28, 34). This can in turn improve our understanding of contemporary plankton-climate feedbacks through the interaction of multiple processes, including ocean-atmosphere exchange of  $\text{CO}_2$ , other greenhouse gases, and aerosol precursors such as DMS (30, 37). Changing EDMS has wide implications for the vulnerable Arctic environment, its human populations, and the weather and climate of lower latitudes (1).

#### Methods

**Remote sensing algorithms.** Daily level 3 composites of remote sensing reflectance spectra acquired by SeaWiFS and MODIS-Aqua were used to retrieve Chl and euphotic layer depth (Zeu) (along with absorption coefficients of colored detrital matter ( $a_{\text{CDM}}$  (412))). These data were used as input to the  $\text{DMS}_{\text{SAT}}$  algorithm (17). First, sea-surface  $\text{DMS}_{\text{PT}}$  ( $\text{nmol L}^{-1}$ ) was estimated as a function of chlorophyll *a* (Chl) concentration using two different equations depending on the phytoplankton light exposure regime. Second, sea-surface DMS concentration ( $\text{nmol L}^{-1}$ ) was estimated from  $\text{DMS}_{\text{PT}}$  and photosynthetically available radiation, after binning these variables to 8-day 28km resolution to achieve full coverage. Remotely sensed sea ice concentration (SIC) was used to screen out ice-contaminated pixels ( $\text{SIC} > 10$ ).  $\text{DMS}_{\text{SAT}}$  was calibrated and validated for the Arctic region using in situ DMS and  $\text{DMS}_{\text{PT}}$  data from a public database supplemented with recent datasets.  $\text{DMS}_{\text{SAT}}$  match-ups with in situ DMS yielded similar validation statistics for SeaWiFS and MODIS-Aqua. Detailed information on algorithm tuning, implementation and validation is provided in the SI Appendix.

**DMS sea-air flux.** FDMS was estimated as the product of the sea-air gas transfer coefficient ( $K_{\text{w}}$ ) and the DMS gradient across the sea-air interface

681 using standard gas exchange parameterizations based on wind speed. We  
682 took into account air- and water-side resistance and the effects of SST and  
683 salinity on DMS diffusivity and solubility (SI Appendix, section 4).

684 **Large scale DMS emission (EDMS).** We estimated EDMS by integrating  
685 FDMS over different periods and spatial domains (e.g., zonal bands and  
686 longitude sectors). The 200 m isobath was used to partition EDMS into open-  
687 ocean and continental shelf domains. Within continental shelves, a threshold  
688 of colored detrital matter  $a_{CDM}(412) > 0.25 \text{ m}^{-1}$  was used to screen for riverine  
689 influence. High Arctic summer EDMS, defined as the May-August emission  
690 north of 70°N, was further regionalized into seven longitude sectors (Fig.  
691 4H). The Greenland and Barents seas and the remaining five sectors were  
692 grouped into the Atlantic and non-Atlantic domains, respectively.

693 **Relationship between ice cover and EDMS.** We computed linear least-  
694 squares regressions between EDMS and the percentage of open ocean water  
695 (pixels with  $\leq 10\%$  SIC) for the high Arctic ( $>70^\circ\text{N}$ ) and for three domains  
696 within it: the Atlantic sector, the non-Atlantic sector, and the Central Arctic  
697 basin. Extrapolation to 100% ice-free water gave an estimate of future  
698 EDMS within a given domain, and the sum of extrapolated quantities gave  
699 a pan-Arctic estimate of future EDMS (Fig. 4I). Extrapolation based on the  
700 regression over the entire domain (which yielded  $200 \pm 54 \text{ Gg S}$ , larger  
701 than the sum of domain-specific EDMS estimates) was discarded owing to  
702 uneven ice-free extent (%) and mean FDMS across domains. Uncertainty in  
703 future EDMS was propagated by adding in quadrature the 95% CI of the  
704 extrapolated predictions for each domain. Uncertainty in the fold-change  
705 with respect to present-day EDMS also took into account the uncertainty  
706 in present-day EDMS estimates (2 standard deviations of 2011–2016 mean  
707 EDMS). Slopes obtained from alternative types of regression (type II major  
708 axis) were not significantly different from those obtained from regular linear  
709 least squares. Additional regressions between EDMS and ice-free extent  
710 (million  $\text{km}^2$ ) in smaller longitude sectors are shown in SI Appendix.

711 **Multiyear trends and means.** We computed linear least-squares re-  
712 gression slopes of satellite-diagnosed quantities (e.g., EDMS) over time (in  
713 decades). Regressions were calculated for the entire study period (1998–2016,  
714  $N = 19$  years) and, north of 70°N, for three sub-periods showing distinct  
715 trends. We also calculated mean EDMS during the initial (1998–2003) and  
716 final (2011–2016) six years, which represent the contiguous years with highest  
717 and lowest sea-ice extent, respectively, and without significant trends in sea-  
718 ice extent ( $p > 0.05$ ). Division of regression slopes by the mean EDMS during  
719 1998–2003 yielded relative rates of change ( $\% \text{ decade}^{-1}$ ). To compute 19-

720 year trends we checked the coherence between SeaWiFS and MODIS-Aqua  
721 records between 2003 and 2007, and corrected for small offsets ( $<3.5\%$ ; Fig.  
722 4A) prior to regression analysis.

723 **Uncertainty assessment.** We assessed the sensitivity of EDMS to varia-  
724 tions in input satellite products and algorithm configuration (SI Appendix,  
725 Table S3). This analysis was conducted only for the MODIS-Aqua record,  
726 which largely drives observed temporal trends. The sensitivity tests included  
727 random perturbation of DMS algorithm coefficients, use of alternative Chl  
728 products and gas exchange schemes, and replacement of time-varying DMS  
729 fields by climatologies ( $\text{DMS}_{\text{SAT}}$  and L11).

#### 730 Acknowledgments

731 We thank the NASA Ocean Biology Distributed Active Archive Center  
732 for access to satellite datasets; the European Centre for Medium-Range  
733 Weather Forecasts for access to ERA-Interim; T.S. Bates (NOAA/ PMEL) and  
734 DMS-GO (COST Action 735) for maintenance of the global sea surface  
735  $\text{DMS(P)}$  database. We are indebted with colleagues who provided additional  
736 DMS data: Sohiko Kameyama, Martine Lizotte, Philippe Tortell and Tereza  
737 Járnikova. We thank Eric Rehm and Maxime Benoît-Gagné for IT support;  
738 Betty Croft, Jon Abbatt, Rafel Simó and Salvador Galí for comments on earlier  
739 drafts of the manuscript; and two anonymous reviewers for constructive  
740 comments. We acknowledge funding from the Canada Excellence Research  
741 Chair in Remote Sensing of Canada's New Arctic Frontier (M.B.), the Canada  
742 Research Chair on Ocean Biogeochemistry and Climate and a NSERC Dis-  
743 covery Grant Program and Northern Research Supplement Program (M.L.),  
744 NETCARE (NSERC Climate Change and Atmospheric Research program) and  
745 ArcticNet (The Network of Centres of Excellence of Canada), and AGAUR  
746 (Generalitat de Catalunya) Beatriu de Pinós postdoctoral fellowship program  
747 (M.G.). This is a contribution to the research program of Québec-Océan and  
748 the Takuvik Joint International Laboratory (CNRS-France & Université Laval-  
749 Canada). **Author contributions** M.G. designed the study with input from  
750 all coauthors; E.D. processed primary satellite data; M.G. implemented the  
751  $\text{DMS}_{\text{SAT}}$  algorithm and analyzed data; M.G. wrote the paper with input from  
752 all coauthors. **Competing financial interests** The authors have no competing  
753 financial interests to declare. **Additional information** We provide free access  
754 to  $\text{DMS}_{\text{SAT}}$  algorithm code (<https://github.com/mgalii>) curated in situ datasets  
755 and  $\text{DMS}_{\text{SAT}}$  datasets (<https://doi.org/10.5281/zenodo.3243967>). Additional  
756 requests should be addressed to M.G.

- 757 1. AMAP (2017) *Snow, Water, Ice and Permafrost in the Arctic (SWIPA) 2017*. (Oslo, Norway).
- 758 2. Bélanger S, Babin M, Tremblay J-E (2013) Increasing cloudiness in Arctic dampens the increase  
759 in phytoplankton primary production due to sea ice receding. *Biogeosciences* 10:4087–4101.
- 760 3. Ridley JK, Ringer MA, Sheward RM (2016) The transformation of Arctic clouds with  
761 warming. *Clim Change* 139(2):325–337.
- 762 4. Arrigo KR, van Dijken GL (2011) Secular trends in Arctic Ocean net primary production. *J*  
763 *Geophys Res* 116(C9).
- 764 5. Vancoppenolle M, et al. (2013) Future Arctic Ocean primary productivity from CMIP5  
765 simulations: Uncertain outcome, but consistent mechanisms. *Global Biogeochem Cycles*  
766 27(3):605–619.
- 767 6. Arrigo KR, van Dijken GL (2015) Continued increases in Arctic Ocean primary production.  
768 *Prog Oceanogr* 136:60–70.
- 769 7. Wassmann P, Reigstad M (2011) Future Arctic Ocean Seasonal Ice Zones and Implications  
770 for Pelagic-Benthic Coupling. *Oceanography* 24(3):220–231.
- 771 8. Kahru M, Brotas V, Manzano-Sarabia M, Mitchell BG (2011) Are phytoplankton blooms  
772 occurring earlier in the Arctic? *Glob Chang Biol* 17(4):1733–1739.
- 773 9. Renaud S, Devred E, Babin M (2018) Northward Expansion and Intensification of Phyto-  
774 plankton Growth During the Early Ice-Free Season in Arctic. *Geophys Res Lett* 45:10,590-  
775 10,598.
- 776 10. Neukermans G, Oziel L, Babin M (2018) Increased intrusion of warming Atlantic water  
777 leads to rapid expansion of temperate phytoplankton in the Arctic. *Glob Chang Biol*  
778 24(6):2545–2553.
- 779 11. Li WKW, McLaughlin F a, Lovejoy C, Carmack EC (2009) Smallest algae thrive as the Arctic  
780 Ocean freshens. *Science* (80-) 326(5952):539.
- 781 12. Blais M, et al. (2017) Contrasting interannual changes in phytoplankton productiv-  
782 ity and community structure in the coastal Canadian Arctic Ocean. *Limnol Oceanogr*  
783 62(6):2480–2497.
- 784 13. Simó R (2001) Production of atmospheric sulfur by oceanic plankton: biogeochemical,  
785 ecological and evolutionary links. *Trends Ecol Evol* 16(6):287–294.
- 786 14. Levasseur M (2013) Impact of Arctic meltdown on the microbial cycling of sulphur. *Nat*  
787 *Geosci* 6(9):691–700.
- 788 15. Galí M, Simó R (2010) Occurrence and cycling of dimethylated sulfur compounds in the  
789 Arctic during summer receding of the ice edge. *Mar Chem* 122:105–117.
- 790 16. Lana A, et al. (2011) An updated climatology of surface dimethylsulfide concentrations and  
791 emission fluxes in the global ocean. *Global Biogeochem Cycles* 25:GB1004.
- 792 17. Galí M, Levasseur M, Devred E, Simó R, Babin M (2018) Sea-surface dimethylsulfide (DMS)  
793 concentration from satellite data at global and regional scales. *Biogeosciences* 15:3497–3519.
- 794 18. Becagli S, et al. (2016) Relationships linking primary production, sea ice melting, and biogenic  
795 aerosol in the Arctic. *Atmos Environ* 136:1–15.
- 796 19. Osman MB, et al. (2019) Industrial-era decline in subarctic Atlantic productivity. *Nature*.
- 797 20. Wang S, Elliott S, Maltrud M, Cameron-Smith P (2015) Influence of explicit Phaeocystis  
798 parameterizations on the global distribution of marine dimethyl sulfide. *J Geophys Res*  
799 *Biogeosciences* 120.
- 800 21. Gabric AJ, Qu B, Matrai P, Hirst AC (2005) The simulated response of dimethylsulfide  
801 production in the Arctic Ocean to global warming. *Tellus B* 57(5):391–403.
- 802 22. Jarnikova T, Dacey JW, Lizotte M, Levasseur M, Tortell PD (2018) The distribution of  
803 methylated sulfur compounds, DMS and DMSP, in Canadian Subarctic and Arctic waters  
804 during summer 2015. *Biogeosciences* 15:2449–2465.
- 805 23. Perrette M, Yool A, Quartly GD, Popova EE (2011) Near-ubiquity of ice-edge blooms in the  
806 Arctic. *Biogeosciences* 8(2):515–524.
- 807 24. Leaitch WR, et al. (2013) Dimethyl sulfide control of the clean summertime Arctic aerosol  
808 and cloud. *Elem Sci Anth* 1:17.
- 809 25. Mahmood R, von Salzen K, Norman A-L, Galí M, Levasseur M (2019) Sensitivity of  
810 Arctic sulfate aerosol and clouds to changes in future surface seawater dimethylsulfide  
811 concentrations. *Atmos Chem Phys* 19(19):6419–6435.
- 812 26. Abbatt JPD, et al. (2019) Overview paper: New insights into aerosol and climate in the Arctic.  
813 *Atmos Chem Phys* 19:2527–2560.
- 814 27. Browse J, et al. (2014) The complex response of Arctic aerosol to sea-ice retreat. *Atmos Chem*  
815 *Phys* 14:7543–7557.
- 816 28. Sharma S, et al. (2017) Arctic sea ice melt leads to atmospheric new particle formation.  
817 *Sci Rep* 7(1):3318.
- 818 29. Park K-T, et al. (2017) Observational evidence for the formation of ocean DMS-derived  
819 aerosols during Arctic phytoplankton blooms. *Atmos Chem Phys* 17:9665–9675.
- 820 30. Charlson RJ, Lovelock JE, Andreae MO, Warren SG (1987) Oceanic phytoplankton, atmo-  
821 spheric sulphur, cloud albedo and climate. *Nature* 326:655–661.
- 822 31. Sharma S, et al. (2012) Influence of transport and ocean ice extent on biogenic aerosol sulfur  
823 in the Arctic atmosphere. *J Geophys Res Atmos* 117:D12209.
- 824 32. Shupe MD, Intrieri JM (2004) Cloud Radiative Forcing of the Arctic Surface: The Influence  
825 of Cloud Properties, Surface Albedo, and Solar Zenith Angle. *J Clim* 17(3):616–628.
- 826 33. Mauritsen T, et al. (2011) An Arctic CCN-limited cloud-aerosol regime. *Atmos Chem Phys*  
827 11:165–173.
- 828 34. Carslaw KS, et al. (2013) Large contribution of natural aerosols to uncertainty in indirect  
829 forcing. *Nature* 503(7474):67–71.
- 830 35. Park KT, et al. (2018) Atmospheric DMS in the Arctic Ocean and Its Relation to Phytoplankton  
831 Biomass. *Global Biogeochem Cycles* 32:1–9.
- 832 36. Mungall EL, et al. (2016) Dimethyl sulfide in the summertime Arctic atmosphere: measure-  
833 ments and source sensitivity simulations. *Atmos Chem Phys* 16:6665–6680.
- 834 37. Six KD, et al. (2013) Global warming amplified by reduced sulphur fluxes as a result of ocean  
835 acidification. *Nat Clim Chang* 3(11):975–978.
- 836 38. Grandey BS, Wang C (2015) Enhanced marine sulphur emissions offset global warming and  
837 impact rainfall. *Sci Rep* 5:13055.
- 838 39. Klimont Z, Smith SJ, Cofala J (2013) The last decade of global anthropogenic sulfur dioxide:  
839 2000–2011 emissions. *Environ Res Lett* 8(14003).
- 840 40. Lynch AH, Serreze MC, Cassano EN, Crawford AD, Stroeve J (2016) Linkages between  
841 Arctic summer circulation regimes and regional sea ice anomalies. *J Geophys Res Atmos*  
842 121:7868–7880.